The Predictive Power of Computational Astrophysics as a Discovery Tool
Proceedings IAU Symposium No. 362, 2023
D. Bisikalo, D. Wiebe & C. Boily, eds.
doi:10.1017/S1743921322001338

Fate of escaping orbits in barred galaxies

Debasish Mondal[1,a] **and Tanuka Chattopadhyay**[1,b]

[1]Department of Applied Mathematics, University of Calcutta,
92 A. P. C. Road, Kolkata 700009, India
E-mail: [a]dmappmath_rs@caluniv.ac.in (✉), [b]tchatappmath@caluniv.ac.in

Abstract. In the present work, we have developed a two-dimensional gravitational model of barred galaxies to analyse the fate of escaping stars from the central barred region. For that, the model has been analysed for two different bar profiles viz. strong and weak. Here the phenomena of stellar escape from the central barred region have been studied from the perspective of an open Hamiltonian dynamical system. We observed that the escape routes correspond to the escape basins of the two index-1 saddle points. Our results show that the formation of spiral arms is encouraged for the strong bars. Also, the formation of grand design spirals is more likely for strong bars if they host central super massive black holes (SMBHs). In the absence of central SMBHs, the formation of less-prominent spiral arms is more likely. Again, for weak bars, the formation of inner disc rings is more probable.

Keywords. Galaxy: evolution, Galaxy: kinematics and dynamics, Galaxies: bar, Chaos

1. Introduction

Stellar bars are quite common among the late-type galaxies. Observational studies reveal that bars are found in nearly 70% of the local disc galaxies (Eskridge et al. 2000). These robust stellar bodies are the result of rotational instabilities that arise in the galactic centre due to the density waves radiating from the core. These instabilities redistribute the stellar trajectories to generate a self-stabilising structure in the form of the bar (Bournaud & Combes 2002). Stellar bars have a paramount role behind the dynamical evolution of galaxies (Navarro & Henrard 2001; Ernst & Peters 2014).

Modelling of galaxies with a rotating bar component can be done via conservative or Hamiltonian dynamical systems. More specifically, stellar escapes from the bar ends can be studied from the viewpoint of escape phenomena observed in open Hamiltonian systems. An open Hamiltonian system is a dynamical system where for energies above an escape threshold, the energy shell is non-compact, and as a result a part of the stellar orbits explores (in our case from potential holes to saddles) an infinite part of the position space (Aguirre et al. 2001). In this dynamical set-up, the overall nature of the stellar orbits has categorized into following categories – (i) escaping and (ii) bounded. Bounded orbits are trapped inside the potential interior and exhibit both periodic (more generally quasi-periodic) and chaotic motions. On the other hand, escaping orbits are generally chaotic in nature. Now, the domains of bounded and chaotic motions in the $x-y$ plane have been observed via Poincaré surface section maps (Strogatz 1994) for different escape energies (i.e. energies higher than the escape threshold).

The orbital and escape dynamics of barred galaxies have been studied in the recent past and results are mainly concentrated towards the computation of the chaotic invariant manifolds near the bar ends and their role behind subsequent structure formations (Jung & Zotos 2016). In our work, we studied a two dimensional (2D) gravitational model

© The Author(s), 2023. Published by Cambridge University Press on behalf of International Astronomical Union

https://doi.org/10.1017/S1743921322001338 Published online by Cambridge University Press

of barred galaxies to study the orbital and escape dynamics of stars in the central region and also analysed the fate of escaping stellar orbits for two different bar profiles viz. strong (i.e. cuspy type) and weak (i.e. flat type).

2. Gravitational Model

To study the orbital and escape dynamics in barred galaxies, we developed a four component gravitational model in 2D (i.e. along the plane of the bar). This model consists of – (a) bulge, (ii) bar, (iii) disc and (iv) dark matter halo. In Cartesian coordinates (x, y), for a test particle of unit mass $(m = 1)$, we construct the following quantities –

$$\text{total potential: } \Phi_{\rm t}(x,y) = \Phi_{\rm B}(x,y) + \Phi_{\rm b}(x,y) + \Phi_{\rm d}(x,y) + \Phi_{\rm h}(x,y), \tag{2.1}$$

$$\text{effective potential: } \Phi_{\rm eff}(x,y) = \Phi_{\rm t}(x,y) - \frac{1}{2}\Omega_{\rm b}^2(x^2+y^2), \tag{2.2}$$

$$\text{Hamiltonian: } H(x,y,\dot{x},\dot{y}) = \frac{1}{2}(\dot{x}^2+\dot{y}^2) + \Phi_{\rm eff}(x,y), \tag{2.3}$$

where $\Phi_{\rm B}$, $\Phi_{\rm b}$, $\Phi_{\rm d}$, $\Phi_{\rm h}$ are potentials corresponding to the bulge, bar, disc and dark matter halo respectively, $\vec{\Omega_{\rm b}} \equiv (0, 0, \Omega_{\rm b})$ (in clockwise sense) is the pattern speed of the bar and H is the Hamiltonian of this system. This gravitational model resembles a conservative dynamical system, in that case H is a constant of motion and equivalent to the total energy of the system (E). Hence, the equation of motion in the rotating reference frame of the bar is –

$$\ddot{\vec{r}} = -\vec{\nabla}\Phi_{\rm t} - 2(\vec{\Omega_{\rm b}} \times \dot{\vec{r}}) - \vec{\Omega_{\rm b}} \times (\vec{\Omega_{\rm b}} \times \vec{r}), \tag{2.4}$$

where $\vec{r} \equiv (x, y)$ and $\dot{\vec{r}} \equiv (\dot{x}, \dot{y})$ are position and linear momentum of the test particle at time t respectively, and $\vec{\nabla} \equiv (\frac{\partial}{\partial x}, \frac{\partial}{\partial y})$. Now, the Lagrangian (or equilibrium) points of the system are solutions of –

$$\frac{\partial \Phi_{\rm eff}}{\partial x} = 0, \frac{\partial \Phi_{\rm eff}}{\partial y} = 0. \tag{2.5}$$

Now, forms of the gravitational potentials for the bulge, bar, disc and dark matter halo are –

- Bulge: $\Phi_{\rm B}(x,y) = -\frac{GM_{\rm B}}{\sqrt{x^2+y^2+c_{\rm B}{}^2}}$ (Plummer 1911), where $M_{\rm B}$ is the bulge mass and $c_{\rm B}$ is the scale length.
- Strong Bar (Model 1): $\Phi_{\rm b}(x,y) = -\frac{GM_{\rm b}}{\sqrt{x^2+(\alpha y)^2+c_{\rm b}^2}}$ (Caranicolas 2002), where $M_{\rm b}$ is the bar mass, α is the flattening parameter and $c_{\rm b}$ is the scale length.
- Weak Bar (Model 2): $\Phi_{\rm b}(x,y) = \frac{GM_{\rm b}}{2a}\ \ln(\frac{x-a+\sqrt{(x-a)^2+y^2+c_{\rm b}^2}}{x+a+\sqrt{(x+a)^2+y^2+c_{\rm b}^2}})$ (Jung & Zotos 2015), where $M_{\rm b}$ is the bar mass, a is the semi-major axis length and $c_{\rm b}$ is the scale length.
- Disc: $\Phi_{\rm d}(x,y) = -\frac{GM_{\rm d}}{\sqrt{x^2+y^2+(k+h)^2}}$ (Miyamoto & Nagai 1975), where $M_{\rm d}$ is the disc mass and k, h are the horizontal and vertical scale lengths, respectively.
- Dark matter halo: $\Phi_{\rm h}(x,y) = \frac{v_0^2}{2}\ \ln(x^2+\beta^2y^2+c_{\rm h}^2)$ (Zotos 2012), where v_0 is the circular velocity, β is the flattening parameter and $c_{\rm h}$ is the scale length.

We analysed our gravitational model separately for two different bar profiles, namely – (i) strong bar (model 1) and (ii) weak bar (model 2). Now, without loss of any generality, we set G (gravitational constant) $= 1$ and other parameter values are given in Table 1 (Zotos 2012; Jung & Zotos 2016).

For these parameter values, we adopt the following scaling relations – unit of length: 1 kpc, unit of mass: $2.325 \times 10^7 M_\odot$, unit of time: 0.9778×10^8 yr, unit of velocity:

https://doi.org/10.1017/S1743921322001338 Published online by Cambridge University Press

Table 1. Parameter values.

Parameter	Value	Parameter	Value
$M_{\rm B}$	$9.3 \times 10^9 M_\odot$	$M_{\rm d}$	$162.75 \times 10^9 M_\odot$
$c_{\rm B}$	0.25 kpc	k	3 kpc
$M_{\rm b}$	$81.375 \times 10^9 M_\odot$	h	0.175 kpc
$c_{\rm b}$	1 kpc	v_0	150 km s^{-1}
α	2 kpc	β	1.3 kpc
a	10 kpc	$c_{\rm h}$	20 kpc
$\Omega_{\rm b}$	12.5 km s^{-1} kpc^{-1}		

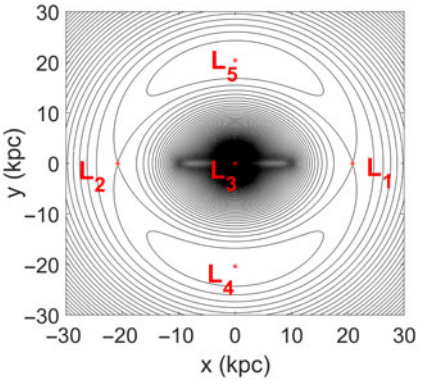

Figure 1. The isocontours of the effective potential—$\Phi_{\rm eff}(x, y)$ in the $x - y$ plane, where locations of the Lagrangian points are marked in red.

10 km s^{-1}, Unit of angular momentum per unit mass: 10 km s^{-1} kpc^{-1} and unit of energy per unit mass: 100 km^2 s^{-2} (Jung & Zotos 2016). Now, from Eqs. 2.5, we calculate the locations of the Lagrangian points for both the strong and weak bar models. In both the models, system has five Lagrangian points, namely L_1, L_2, L_3, L_4 and L_5 (viz. Fig. 1). Among these Lagrangian points only L_1 and L_2 (classified as index-1 saddle points of the system) are corresponding to the bar ends i.e. responsible for stellar escapes. For the strong bar model the locations of L_1 and L_2 are $(\pm 20.23113677, 0)$ respectively, and for the weak bar model that locations are $(\pm 20.82978638, 0)$. Clearly, the bar area of model 2 is bigger than the model 1.

3. Computational Results

The effective potential term ($\Phi_{\rm eff}$) (viz. Eq. 2.1) is symmetric about the y axis and $E_{L_1} = E_{L_2}$, where E_{L_1} and E_{L_2} denotes the energy values of L_1 and L_2 respectively. Hence, studying the dynamics near either of L_1 and L_2 is sufficient to analyse the system. Now, escape of stars from the central barred region is only possible in the energy range: $E > E_{L_1}$, and for $E \leqslant E_{L_1}$ orbits are bounded inside the central barred region. To study the escaping motion, we integrate the Eq. 2.4 for a time-scale of 10^2 time units, which is equivalent to 10 Gyr i.e. the typical age of the bars (James & Percival 2018). For this orbit integration we use the `ode45` package of `MATLAB`. Further, in order to simplify the calculations, we adopt the dimensionless energy parameter $C = \frac{E_{L_1} - E}{E_{L_1}}$ (Jung & Zotos 2016). Hence, orbital escapes are possible for $C > 0$.

3.1. *2D Orbits*

To study the nature of orbits near the Lagrangian point L_1 for both the bar models, we choose an initial condition $x_0 = 10$, $y_0 = 0$, $\dot{x}_0 = 15$, where $\dot{y}_0$ is evaluated from Eq. 2.3, and the corresponding trajectories in the $x - y$ plane are drawn for several values of $C > 0$

https://doi.org/10.1017/S1743921322001338 Published online by Cambridge University Press

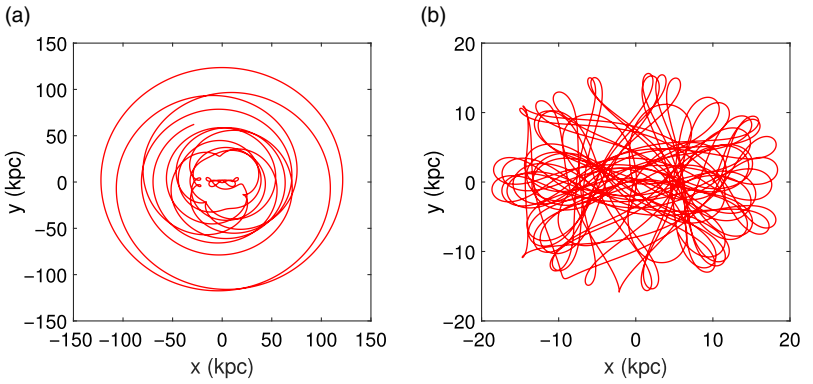

Model 1—escaping chaotic orbit. Model 2—non-escaping chaotic orbit.

Figure 2. Orbits in the $x-y$ plane for $(x_0, y_0, \dot{x}_0) \equiv (10, 0, 15)$ and $C = 0.1$.

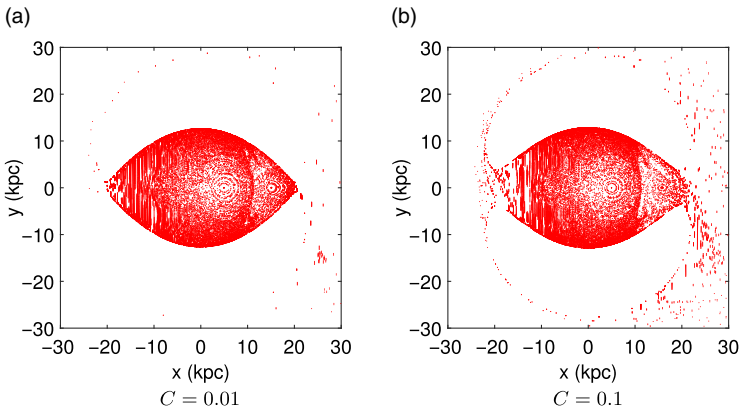

$C = 0.01$ $C = 0.1$

Figure 3. Model 1—Poincaré surface sections of $\dot{x} = 0$ and $\dot{y} \leqslant 0$.

(see Fig. 2). Any other initial condition in the suitable neighbourhoods of the aforesaid initial condition will follow the similar trend.

3.2. *Poincaré Maps*

Poincaré surface section maps in the $x-y$ plane for both the bar models are shown in Fig. 3 and Fig. 4 for several values of $C > 0$. In order to construct the Poincaré surface section maps, we choose a 43×43 gird of initial conditions i.e. (x_0, y_0) in the $x-y$ plane with restriction: $(x_0^2 + y_0^2) < r_{L_1}^2$, where r_{L_1} is the radial length of L_1. Also, $\dot{x}_0 = 0$ and $\dot{y}_0 (> 0)$ is evaluated from Eq. 2.3. In these maps our chosen surface cross sections are $\dot{x} = 0$ and $\dot{y} \leq 0$.

4. Conclusions

From all the above analyses our findings are –

• Model 1 (strong bar): For galaxies with strong bars, escape of stars from the central region has been encouraged (Fig. 2(a)). Again, the amount of escape from the bar ends has been increased with increment in the escape energy (Figs. 3(a) and 3(b)). Hence, for strong bars, the formation of spiral arms is more likely as a result of escape. Here, the increment in escape for higher escape energy values have been interpreted by the violence (viz. baryonic feedbacks from supernova, shocks etc.) occurring in the central region (Melia & Falcke 2001). We know, the central black hole has a strong influence on

https://doi.org/10.1017/S1743921322001338 Published online by Cambridge University Press

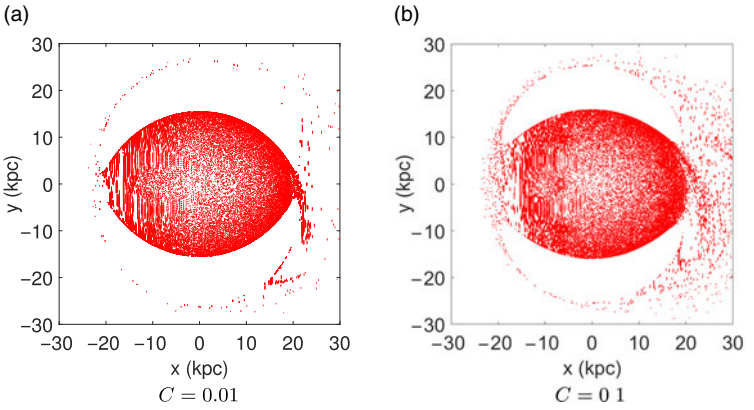

Figure 4. Model 2—Poincaré surface sections of $\dot{x} = 0$ and $\dot{y} \leqslant 0$.

the kinetic energy of random motions inside the bulge due to the central violence. Further, these kinetic energy of random motions is strongly related with spiral arm strength (Al-Baidhany et al. 2014). Galaxies with central Super Massive Black Holes (SMBHs) have more kinetic energy of random motions inside the bulge and spiral arms with small pitch angles (Seigar et al. 2008). Hence, for strong barred galaxies with central SMBHs, the formation of tightly wound or full-fledged spiral arms is more likely. This is the case of giant spiral galaxies, where grand design spiral arms are observed. Few examples of such giant spiral galaxies are Milky Way, NGC 1300 (Helou et al. 1991) etc. While, in the absence of central SMBHs, galaxies have competitively lesser kinetic energy of random motions inside the bulge and spiral arms with competitively higher pitch angles. Hence, for strong barred galaxies without central SMBHs, the formation of less prominent spiral arms is more likely.

• Model 2 (weak bar): For galaxies with weak bars, escape of stars from the central region has not been encouraged (Fig. 2(b)). Here also, the amount of escape from the bar ends has been increased with increment in the escape energy (Figs. 4(a) and 4(b)). Hence, for weak bars, the formation of inner disc rings is more likely as a result of escape. While, the increment in violence occurring in the central region may strengthen the ring patterns. Hence, for weak barred galaxies, the formation of inner disc rings is more likely. Few examples of such ring galaxies are NGC 1533, NGC 6028 (Helou et al. 1991) etc.

References

Aguirre, J., Vallejo, J. C., Sanjuán, M. A. F. 2001, *Phys. Rev. E*, 64, 066208
Al-Baidhany, I., Seigar, M., Treuthardt, P., *et al.* 2014, *J. Ark. Acad. Sci.*, 68, 25
Bournaud, F., Combes, F. 2002, *A&A*, 392, 83
Caranicolas, N. D. 2002, *J. Astrophys. Astron.*, 23, 173
Ernst, A., Peters, T. 2014, *MNRAS*, 443, 2579
Eskridge, P. B., Frogel, J. A., Pogge, R. W., *et al.* 2000, *AJ*, 119, 536
Helou, G., Madore, B. F., Schmitz, M., *et al.* 1991, *Databases & On-Line Data in Astronomy*, 171, 89
James, P. A., Percival, S. M. 2018, *MNRAS*, 474, 3101
Jung, C., Zotos, E. E. 2015, *PASA*, 32, e042
Jung, C., Zotos, E. E. 2016, *MNRAS*, 457, 2583
Melia, F., Falcke, H. 2001, *ARA&A*, 39, 309
Miyamoto, M., Nagai, R. 1975, *PASJ*, 27, 533
Navarro, J. F., Henrard, J. 2001, *A&A*, 369, 1112
Plummer, H. C. 1911, *MNRAS*, 71, 460

https://doi.org/10.1017/S1743921322001338 Published online by Cambridge University Press

Seigar, M. S., Kennefick, D., Kennefick, J., Lacy, C. H. 2008, *ApJ*, 678, L93
Strogatz, S. H. 1994, *Nonlinear Dynamics and Chaos: With Applications to Physics, Biology, Chemistry, and Engineering*, Addison-Wesley
Zotos, E. E. 2012, *Res. Astron. Astrophys.*, 12, 500

Discussion

MELLEMA: Question: The rotation pattern of the bar does not affect the position of resonances, bar mass etc. Could you comment on this?
Answer: Here we only consider a fixed bar pattern speed and focus completely on the overall nature of stellar escapes for different bar types. In our upcoming works, we are planning to study the effect of the bar pattern speed on the position of bar resonances, bar mass etc. to classify the stellar orbits under different bar types.
Question: What will be the outcome if the system has more than one pattern speed?
Answer: If the system has more than one bar pattern speed, then in general the potential becomes time-dependent. So, the system becomes non-conservative and our Hamiltonian approach fails. In that case, we can still use our Hamiltonian approach, if both the bars are aligned perpendicularly to each other and have the same pattern speed.

https://doi.org/10.1017/S1743921322001338 Published online by Cambridge University Press